Colloidal Gold Particles as an Incompressible Atomic Force Microscope Imaging Standard for Assessing the Compressibility of Biomolecules

James Vesenka,* Srinivas Manne,‡ Richard Giberson,§ Thomas Marsh,* and Eric Henderson*
*Iowa State University, Department of Zoology and Genetics, Ames, Iowa 50010; ‡University of California, Department of Physics, Santa Barbara, California 93106; §Ted Pella Inc., Research and Development, Redding, California 96003 USA

ABSTRACT Colloidal gold particles have multiple uses as three-dimensional atomic force microscopy imaging standards because they are incompressible, monodisperse, and spherical. The spherical nature of the particles can be exploited to characterize scanning tip geometry. As uniform spheres, colloidal gold particles may be used to calibrate the vertical dimensions of atomic force microscopy at the nanometer level. The monodisperse and incompressible nature of the gold can be used to characterize the vertical dimensions of coadsorbed biomolecules. Simultaneous measurements of gold with tobacco mosaic virus show that, at the same applied vertical force, the tobacco mosaic virus is undamaged by blunt tips but is compressed or disintegrated under sharper scanning styli, suggesting that specimen degradation is partly a pressure-dependent effect.

INTRODUCTION

The atomic force microscope (AFM) is essentially a high resolution profilometer, capable of resolving atomic dimensions (Binnig et al., 1986). The basic operational principle involves the response of an extremely sharp probe to highly localized forces between the probe and sample. The probe is usually attached to a flexible cantilever that is deflected as it responds to the forces between the specimen and the probe. These deflections can be monitored optically and/or electronically, and the output is digitized and recorded on a computer.

Compared to electron microscopy, the two most significant advantages of this technique are the ability of the AFM to obtain real-time three-dimensional images (Binnig et al., 1986) and to image under fluids (Drake et al., 1989, Hansma et al., 1992a; Henderson et al., 1992). Reliable length measurements of double-stranded DNA have been reported by several authors (Bustamante et al., 1992; Hansma et al., 1992b; Lyubchenko et al., 1992; Vesenka et al., 1992a). However, the complex nature of the forces between the tip and sample makes it difficult to obtain reliable height information of the imaged specimen, especially at the nanometer scale (Li and Lindsay, 1991; Maivald et al., 1991). It is suspected that biomolecules may be compressed by the scanning stylus, distorting the specimen dimensions (Engel, 1991; Bustamante et al., 1992; Radmacher et al., 1992) or be partially buried in the dried buffer layer (Lyubchenko et al., 1993; Vesenka et al., submitted for publication). For example, images of DNA in air have been reported by some authors to have heights of less than 1 nm (Bustamante et al., 1992; Vesenka et al., 1992a; Lyubchenko et al., 1993; Shaiu et al., 1993b), less than 50% of the expected value.

One solution to the problem of obtaining reliable height information from the atomic force microscope is to use colloidal gold particles. These can be fabricated by a number of different methods (Frens, 1973; Mühlpfordt, 1982; Baschong et al., 1985; Slot and Geuze, 1985). In these processes, stable gold spheres are generated between 10 and 20 nm in diameter, and monodispersity can be achieved through separation of particle sizes by centrifugation (DeMey, 1984). Some authors have employed immuno-labeled gold as markers in AFM imaging (Shaiu et al., 1993a; Putman et al., 1992, 1993). The spherical nature of the gold particles can be exploited to characterize the scanning probe geometry, i.e., tip shape (Putman et al., 1993; Vesenka et al., submitted for publication) and sharpness. Their monodispersity may be used to calibrate the vertical scale of piezoelectric response. Colloidal gold particles have a decisive advantage in tip characterization when compared with highly uniform biomolecules (Thundat et al., 1992a). The particles, as shown in this study, are incompressible, whereas the biomolecules are not.

Because AFM is a near field contact microscopy, perhaps the most significant application of colloidal gold particles is to address the problem of specimen compressibility and damage by the scanning tip. The primary interest of this paper is to show that gold particles, when coadsorbed with biomolecules, can be used to assess tip-induced deformations in the biomolecular structure that otherwise might be attributed to other instrumentation or specimen preparation procedures. To do this we first estimate the tip shape from the independently characterized spherical nature of the gold particles. Then we show the gold particles are incompressible and can be employed to obtain reliable height information. With this information we can quantitatively assess the compressibility of tobacco mosaic virus coadsorbed with 10-nm colloidal gold particles.

MATERIALS AND METHODS

AFM specimen preparation

Twenty μl of spermine (Sigma Chemical Co., St. Louis, MO) was adsorbed onto freshly cleaved mica for 10 s and immediately rinsed with 1 ml of distilled/deionized water (ddH_2O) followed by thorough drying in nitrogen and storage in a dessicator. It is likely that the polyamine imparts a net positive charge that facilitates gold and biomolecule attachment. Fresh,

Received for publication 7 December 1992 and in final form 28 May 1993.
Address reprint requests to Dr. J. Vesenka.

0006-3495/93/09/992/06 $2.00

monodisperse colloidal gold particles (5, 10, 16, 20, and 24 nm) were prepared from standard reduction processes (DeMey, 1984) without stabilizers (Ted Pella, Redding, CA, 0.01% gold by weight). The gold was diluted 1:10 in ddH_20, adsorbed onto the treated mica for 5 min, rinsed with 1 ml of ddH_20, and thoroughly dried in nitrogen. Tobacco mosaic virus (TMV; gift from Allen Miller, Iowa State University), a helical RNA virus 18 nm in diameter and 300 nm long (Mathews, 1981), was mixed with colloidal gold in a buffer of 100 mM K_2PO_4 and 10 mM $MgCl_2$ and was adsorbed to treated mica in the same manner that the gold was attached.

The specimens were imaged in air with Nanoscope II and Nanoscope III atomic force microscopes (Digital Instruments, Santa Barbara, CA) in the repulsive contact imaging mode at forces of less than 20 nN. The lateral dimensions of the piezo were calibrated with a 2160-lines/mm square grating (Ted Pella, Redding, CA) and the vertical dimensions were calibrated with colloidal gold particles (see Results and Discussion). The flattened raw data was gathered and presented in 512 × 512 pixel format over representative 2x2-μm^2 areas (about 4 × 4 nm^2/pixel). The mean vertical surface roughness of the spermine-treated mica is less than 1 nm over 0.5- × 0.5-μm^2 sample areas. This treatment contributes an error in the height measurements of the gold and TMV of less than 10%. Both the colloidal gold particles and TMV specimens were imaged under reduced humidity (8%) for stable imaging (Vesenka et al., 1992a; Thundat et al., 1992b). Samples were imaged with silicon nitride or silicon tips (Digital Instruments, Santa Barbara, CA, and Park Scientific, Mountainview, CA) with several spring constants (0.03–0.6 nN/nm) and radii of curvature (6–130 nm). The direction of scan with respect to the cantilever (scan orientation) was adjusted until the forward and reverse traces superimposed (Lyubchenko et al., 1993; Shaiu et al., 1993a, 1993b), an optimal imaging condition that negates the apparent height contribution due to frictional effects between the tip and sample (Radmacher et al., 1992, Zenhausern, 1992a).

TEM specimen preparation

Transmission electron microscopy of the gold and TMV were performed with a JEOL JEM 100 CX II TEM at 80 kV and 50,000 × magnification calibrated with a 2160 lines/mm grating. Carbon-coated formvar (Polysciences, Warrington, PA) was glow-discharged, and samples of gold and TMV were negatively stained with 2% uranyl acetate. Analysis of height and widths (base to base) from the AFM images was carried out on the Nanoscope software. Width measurements of the TEM images were accomplished with a profile projector. Transmission electron microscopy of the AFM tip profiles was accomplished with a JEOL JEM 1200 CX at 80 kV and magnifications at 10,000 and 200,000 ×. All data was statistically analyzed and plotted using Kaleidagraph software (Synergy Software, Reading, PA).

RESULTS AND DISCUSSION

Fig. 1 is an AFM image of 10- and 24-nm colloidal gold particles and a transmission electron micrograph (TEM) of the tip that imaged these particles. Fig. 2 *a* is a plot of heights (H) and widths (W) from the data taken in Fig. 1 *a*. Fig. 2 *b* is a model used to relate H and W to the radius of curvature of the tip (R_c). Fig. 2 *c* compares TEM R_c and AFM R_c for six different tips. The central purpose of the model proposed in Fig. 2 is to provide a quick method for estimating the tip curvature. This model is based on empirical evidence that suggests the AFM images are composed of the desired specimen and substrate binding material (spermine).

For all the tips imaged with a TEM in this study, the end radii were reliably approximated by hemispheres, as with the tip in Fig. 1 *b* having an $R_c = 17 \pm 2$ nm. Fig. 2 *b* is a two-dimensional model of a hemispherical tip in contact with the specimen hemisphere of radius H (details discussed below). The two hemispheres have colinear radii that form an angle ϕ with the normal to the specimen surface. The relationship between W, R_c, H, and ϕ is given by

$$\frac{W}{2} = R_c \sin \phi + H \sin \phi. \quad (1)$$

A plot of W versus H yields a slope 2 sin ϕ and an intercept of $2R_c$ sin ϕ, enabling the simultaneous solution of ϕ and R_c from a linear fit to the data. For example, in the data shown in Fig. 2 *a*, $W = 33.0 + 1.89H$. This corresponds to $\phi = 71 \pm 18°$ and $R_c \approx 17 \pm 4$ nm, which is in excellent agreement with the observed tip radius of 17 ± 2 nm. R_c and ϕ are also related by

$$\cos \phi = \frac{R_c}{R_c + H}. \quad (2)$$

Since these contact angles depend on the height of the imaged specimen, we expect $\phi_{10nm} = 66°$ and $\phi_{24nm} = 51°$ based

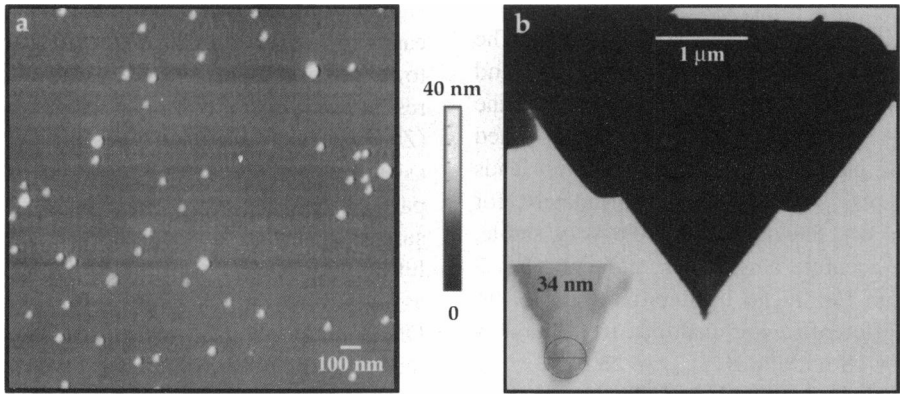

FIGURE 1 (*a*) Nominal, 10- and 24-nm colloidal gold particles imaged with a commercial "oxide-tip" AFM probe at a total force of about 35 nN. TEM characterization of the particles yields diameters 10.0 ± 1.2 nm ($N = 100$) and 24.2 ± 1.9 nm ($N = 100$), compared to AFM height characterization of 9.8 ± 1.1 nm ($N = 100$) and 23.0 ± 3.6 nm ($N = 116$). The vertical gray scale shows taller features in lighter color and darker features as the background level of the image. (*b*) A TEM profile image of the AFM tip used in *a*, with a high magnification inset of the tip's apex. The solid bar on the top of the larger image is the cantilever. The commercial cantilever has a radius of curvature of about 17 nm as estimated by the sphere superimposed on the inset tip.

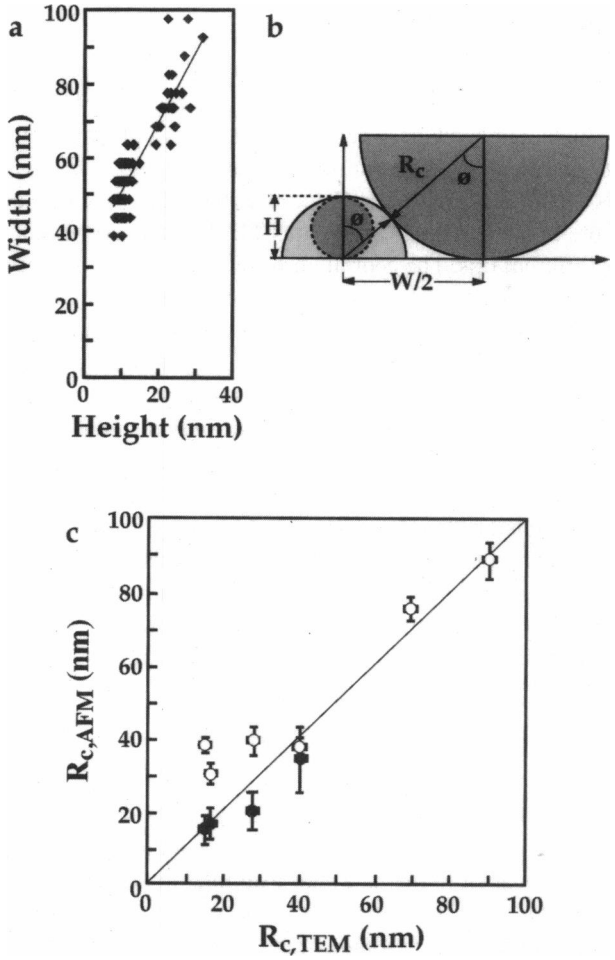

FIGURE 2 (*a*) A plot of the height and width from 100 colloidal particles imaged by the tip shown in Fig. 1 *b*. (*b*) A model describing the image width as the result of two interacting incompressible hemispheres. (*c*) Plots of the diameters of AFM estimates versus TEM measurements of the tip radii. The diagonal in the graph is the ideal condition of both measurements in agreement. The open circles represent estimates from Eq. 2. Eq. 2 yields poor approximations for tip radii having similar dimensions to the colloidal gold particles. The closed circles represent the estimate from Eq. 1 for smaller radii tips.

on Eq. 2 and R_c independently characterized by TEM. The discrepancy between the angles generated from Eqs. 1 and 2 can be attributed to the significant amount of scatter in the width measurements (Fig. 2 *a*). This problem is associated with polydispersity of the gold colloid and sometimes leads to unphysical intercepts, i.e., $\sin\phi > 1$. Fortunately, for sharper tips (smaller W), the intercepts were very stable, reflecting the highly accurate height measurements. Eq. 2 and the intercept from Eq. 1 can be iteratively solved to approximate R_c for different H. For example, from the data in Fig. 1 *a*, $R_{c,10nm} \approx 18$ nm and $R_{c,24nm} \approx 23$ nm.

The data scatter leads to degradation of the slope and intercept for blunt tips (large W), leading to nonphysical values of the angle ϕ and R_c. Under these conditions we ignore the contribution of the width due to $2H \sin\phi$. Instead we use $R_c \sin\phi \approx \sqrt{2HR_c}$ and Eq. 1 to obtain the squared approximation for W (Vesenka et al., 1992a; Zenhausern et al., 1992b):

$$W^2 \approx 8R_cH. \quad (3)$$

A plot of colloidal gold W^2 versus H yields a slope of $8R_c$. Fig. 2 *c* includes estimates of the radius of curvature based on Eq. 1 (when possible) and Eq. 3 for six data sets. The parabolic approximation, although accurate for electron beam deposited tips for imaging steep walled geometries (Keller, 1992), was unnecessary in our case since the R_c was much greater than the height of the imaged specimen. The major difficulty in characterizing a given tip geometry comes from the time-consuming labor involved in taking geometric measurements of the gold particles from AFM images. Presumably, this difficulty can be alleviated in future analysis with appropriate software automation.

By assuming a hemisphere for the sample rather than a sphere, as would be expected intuitively, we are attempting to account for potential sources of ellipticity in the sample. This ellipticity may be due to either asymmetry of the colloidal gold particles or buildup of substrate binding matter around the gold. The former should be a random event, since the gold will spread out on the AFM surface in arbitrary orientations. The latter effect might be caused by migration of the highly positively charged spermine groups to the highly negatively charged, unstabilized colloidal gold particles. Fig. 2 *b* addresses this problem by assuming the colloidal gold particle is a sphere (*dotted circle*) encased in the substrate binding matter (*lighter hemisphere*). The assumption of a hemisphere for an imaging target is driven by AFM image evidence that suggests the spheres have some buildup of substrate binding matter, as can be seen when colloidal particles are pushed off their pedestals at high forces (data not shown). The hemispherical assumption is further supported by empirical evidence of intercepts that are between 1 and 2 from W versus H plots. This would yield nonphysical results if the same trigonometric analysis were applied to the spherical specimen in Fig. 2 *b*.

We emphasize that the model proposed in Fig. 2 *b* is designed to obtain a rough approximation of tip shape from easily measured height and width parameters. It is not meant to supplant the known ability of the AFM to obtain atomic resolution, a likely consequence of apical atomic asperities (Zasadzinski et al., 1991; Vesenka et al., 1992b). A basic assumption in the model proposed in Fig. 2 *b* is that the particles are not compressed by an AFM probe. This assumption plays a key role in the development of deconvolution algorithms and the application of the colloidal particles as a reliable height standard with coadsorbed biomolecules. Once the tip shape is known, a coadsorbed biological specimen might be deconvolved along the contour of the specimen that is contacted by the tip. Surface topography not contacted by the tip due to exclusion by tip-sample interaction would still remain indeterminate (Keller, 1992).

Fig. 3 *a* plots the colloidal gold particle heights versus normal force for a cantilever with a quoted spring constant

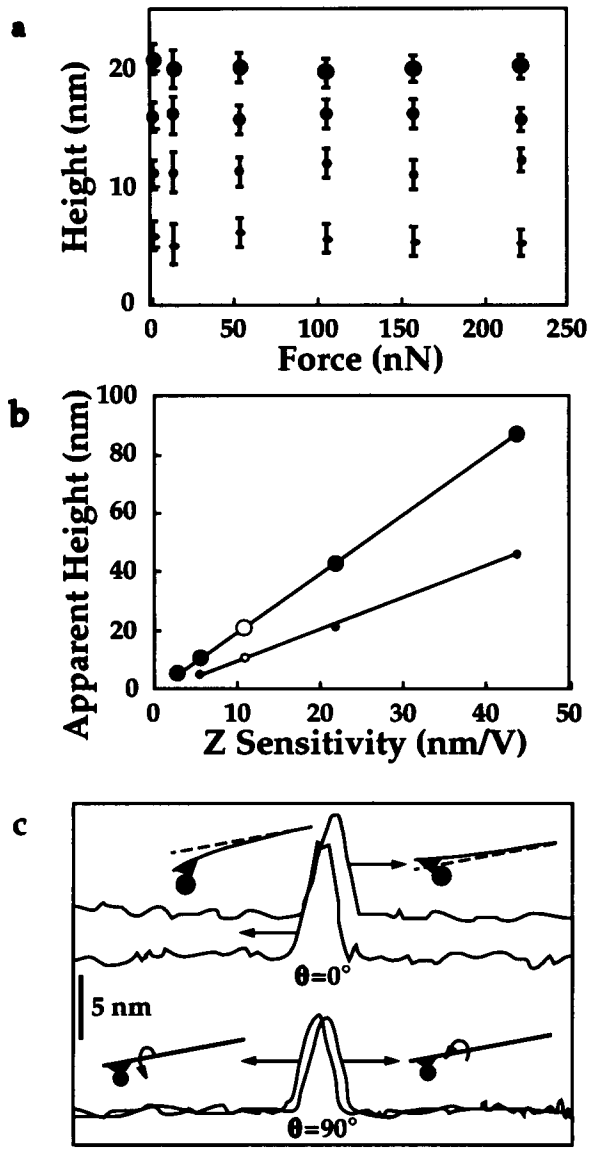

FIGURE 3 (*a*) A plot of colloidal gold incompressibility (N = 50 each) as a function of repulsive contact force (increasing *sizes* of *dots* represent, respectively, 5, 10, 16, and 20 nm) from a cantilever with spring constant of 0.6 nN/nm and $R_c \approx 45$ nm estimated by Eq. 1. (*b*) A plot of apparent colloidal gold particle height versus *z*-piezo sensitivity for 20 nm (*large solid circles*) and 10 nm (*small solid circles*) particles. The open circles represent the calibrated height of the piezo at the appropriate *z*-piezo sensitivity. (*c*) Effect on image height of an 8-nm colloidal gold particle imaged at scan angles of 0 and 90°. At $\theta = 0°$, Δ | $\text{Height}_{\text{Trace-Retrace}}$ | = 1.4 ± 0.4 nm, and at $\theta = 90°$, Δ | $\text{Height}_{\text{Trace-Retrace}}$ | = 0.2 ± 0.4 nm. At 0 and 180° the tip height is subject to increase or decrease due to frictional effects, but at 90 and 270° this effect is minimized and the traces frequently are superimposable.

of 0.6 N/m, one of the stiffest commercially available. Although there is tremendous variation in the experimental spring constants (Cleveland et al., 1993), by using a stiff cantilever we are assured of exerting a repulsive "Hookean" force (Lyubchenko et al., 1993) larger than typically used for imaging biomolecules (Bustamante et al., 1992; Hansma et al., 1992a). Within experimental error there was no noticeable decrease in height of the colloidal gold, indicating that the particles are incompressible. Fig. 3 *b* shows the apparent height of 10- and 20-nm gold particles at several *z*-piezo sensitivities for the purpose of checking the vertical calibration. The slopes of the two curves are 2.0 V/nm (20-nm size) and 1.1 V/nm (10-nm size), giving a slope ratio of 1.8:1, which is in excellent agreement with the 2:1 ratio of size between the larger and smaller particles independently characterized by electron microscopy (data not shown).

Height measurements of all images were taken from scans that had the least amount of height distortion between the trace and retrace when the laser beam centered over the tip end (Lyubchenko et al., 1993; Shaiu et al., 1993a, 1993b). Under these conditions the scan angle was usually around 90°, when the direction of the scan is parallel to the edge of the glass substrate to which the cantilever is attached. Height distortion has been attributed to frictional effects (Radmacher et al., 1992; Zenhausern et al., 1992a). In Fig. 3 *c* we show trace and retrace images of an 8-nm colloidal gold particle being imaged perpendicular to the substrate's short end (0°) and parallel to the substrate's short end (90°) by a cantilever with a quoted spring constant of 0.06 N/meter. Notice at the 0° scan angle that the left to right trace has a shorter height than the right to left trace by about 1.4 ± 0.4 nm, as measured from the baseline. The height difference is likely due to frictional effects when the tip contacts the gold particles at scanning directions normal to the cantilever substrate (Radmacher et al., 1992), as schematically outlined in the deviation from the true height (*dotted line*) in the cartoon cantilevers. When the scan direction is approximately 90 or 270°, the torsion on the tip contributes negligibly to the height difference. When cantilevers with stiffer spring constants were used, the height anomalies were reduced dramatically, confirming theoretical predictions proposed by other authors (R. J. Warmack, X-Y. Zheng, T. Thundat, and D. P. Allison, submitted for publication).

Because the gold particles are incompressible and reflect dimensions that can be independently characterized through electron microscopy, they make useful incompressible standards to assess tip-sample interactions with coadsorbed biomolecules. 10-nm colloidal gold particles were dried onto spermine-treated mica with TMV. Fig. 4 shows a comparison among a TEM and three AFM images of 10-nm gold particles coadsorbed with TMV. The inset in each image is a statistical plot of either widths (TEM in Fig. 4 *a*) or heights (AFM in Fig. 4, *b–d*) of the gold particles and TMV. The electron micrograph in 4 *a* yields similar distributions of gold particles and TMV as the AFM image in 4 *b*, which was taken with a 60 nm R_c tip at 16 nN. The TMV distributions are narrower than the gold for both techniques, which is expected since the viral molecules are much more uniform than the man-made colloidal gold particles.

Fig. 4 *c* shows the consequence of imaging the coadsorbed species with a moderately sharp tip ($R_c \approx 26$ nm estimated by Eq. 1) at 8 nN of force. Notice that the average height and distribution width of the gold particles remains unchanged

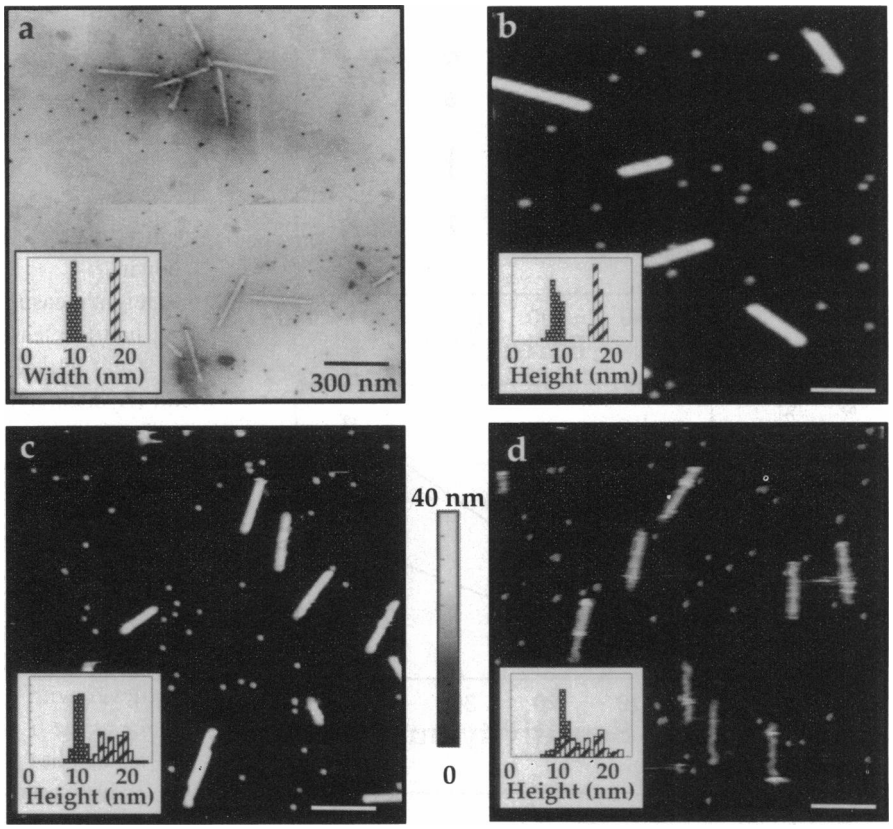

FIGURE 4 A plot of TEM and AFM colloidal gold/TMV specimens with diameter/height statistics. The length marker in *a* of 300 nm is the same for all four images. (*a*) A transmission electron micrograph of 10-nm gold/TMV prepared on a carbon-coated EM grid. The statistical distribution of 101 particle and TMV *widths* is plotted to its right (gold: 9.9 ± 1.0 nm, TMV: 18.2 ± 0.4 nm). (*b*) An atomic force image of 10-nm gold/TMV imaged by a dull tip with $R_c \approx 57$ nm at a probe force ≈ 16 nN. The inset includes a statistical distribution of 101 particle and TMV *heights* (gold: 9.3 ± 1.0 nm, TMV: 18.0 ± 0.8 nm). (*c*) A display of an AFM image of colloidal gold/TMV with 101 height statistics for a tip of intermediate $R_c \approx 26$ nm at 8-nN loading force (gold: 9.9 ± 0.9 nm, TMV: 17.3 ± 2.4 nm). (*d*) A sharp tip of $R_c \approx 6$ nm at a probe force ≈ 17 nN with the height statistics for the gold and TMV in the inset (gold: 10.0 ± 1.5 nm, TMV: 14.2 ± 3.8 nm). The sharp tip seems to tear the TMV, while the gold remains unaffected by imaging in the repulsive contact mode. The TMV height statistics confirm this result, being narrow for the fat tip and varied for the thin tip. We can estimate the normal pressure exerted by the probe on the TMV as the scanning force divided by the contact area approximated from the tip radius of curvature. The pressure on the TMV in *b* is 0.35 MPa, in *c* the normal pressure is 0.94 MPa, and in *d* the normal pressure is 42 MPa.

(mean and standard deviation = 9.9 ± 0.9 nm), but the average height of the TMV has decreased somewhat and the width of the distribution has increased significantly (17.3 ± 2.4 nm). When the normal loading force was reduced to the minimal breakaway force, the average height returned to the expected 18 nm (data not shown). Fig. 4 *d* is an example of imaging gold and TMV with a sharper tip ($R_c \approx 6$ nm estimated by Eq. 1) at a force of 19 nN. Again, the colloidal gold particles have consistent height and distribution width (10.0 ± 1.3), but the TMV has been irreversibly damaged by the sharper tip (14.2 ± 3.8 nm). We estimate the pressure at which the onset of compression occurs to be about 1 MPa (cf. Fig. 4 caption for details). These data suggest that compression by the tip occurs as the tip radius decreases until irreversible damage is inflicted upon the specimen.

In our studies there was no distinction between total force, both Hookean and capillary, or capillary force alone on biomolecule sample widths, as has been observed elsewhere (Yang and Shao, 1993). Several different phenomena associated with the tips and cantilevers might explain this result, including 1) tip chemistry, 2) tip roughness, 3) shear due to cantilever stiffness, and 4) increased pressure on the specimen due to reduction of the tip area. It is possible that tip chemistry or tip roughness could generate conditions that might damage the biomolecules. In these studies the effect of tip chemistry is ruled out, because only silicon nitride tips were used; thus, the tip-sample interaction is the same for all images. Tip roughness could be addressed by taking high resolution transmission electron micrographs of the probe to examine the tip geometry. However, as can be seen in Fig. 1 *b*, such analysis has not been profitable, because charge build-up on the insulating silicon nitride cantilevers makes high resolution difficult. We are presently testing the importance of both tip chemistry and shape by repeating these experiments with carbonaceous electron beam deposited tips (Keller and Chih-Chung, 1992) which are conducting and are more easily characterized by electron microscopy (Akama et al., 1990).

The error signal, i.e., part of the cantilever deflection not compensated by the feedback loop (Putman et al., 1992), may play an important role in sample damage as larger spring constants can contribute greater shear stress to the biomolecules. When blunt tips with stiff cantilevers were used to image the specimen at the same force and scan settings as in Fig. 4 (data not shown), no roughening of the TMV was detected. However, with the sharper tips used in Fig. 4, *c* and *d*, the normal pressure increased, with a concomitant increase in lateral pressure, causing the TMV to disintegrate. Since the range of forces in air is usually not less than 1 nN, obtaining higher resolution of biomolecules with sharper tips will require other mechanisms of force abatement, e.g., by working in fluids (Drake et al., 1989) or employing improved noncontact imaging methods (Giles et al., 1993).

SUMMARY

We have provided evidence that monodisperse colloidal gold makes a useful atomic force microscopy imaging standard

for estimating the scanning tip geometry and for calibrating the vertical scale of the scanning piezoelectric transducer on the nanometer scale. Comparison of AFM images of colloidal gold particles coadsorbed with tobacco mosaic virus obtained with blunt and sharp tips suggests that sample damage may be a pressure-dependent effect. Thus, improved resolution in air may occur at the expense of potentially greater injury to the specimen. The incompressible nature of the colloidal gold particles should make them useful for determining the compression of coadsorbed biomolecules.

We thank Richard Miller for his helpful discussions, Jack Horner and Bruce Wagner for the use of the Bessey Electron Microscopy Facility, and Dan Jondle, John Weber, and Erin Aten for their assistance with data taking and proofreading of the manuscript. We also thank Stephen Kowalczykowski at the University of California, Davis, for the use of his laboratory during the exploratory investigations and Dr. John Chandler of Cardiff, Wales, for monodisperse colloidal gold preparations.

The work is supported by an AT&T fellowship (to S. Manne), National Science Foundation (NSF) grant DIR-9113593 (to Philip G. Haydon), NSF grant DIR-9004649, and National Institutes of Health grant GM41899 (to E. Henderson).

REFERENCES

Akama, Y., E. Nishimura, A. Sakai, and H. Murakami. 1990. New scanning tunneling microscopy tip for measuring surface topography. *J. Vac. Sci. Technol. A.* 8:429–433.

Baschong, W., J. M. Lucocq, and J. Roth. 1985. "Thiocyanate gold": small (2–3 nm) colloidal gold for affinity cytochemical labeling in electron microscopy. *Histochemistry.* 83:409–411.

Binnig, G., C. F. Quate, and Ch. Gerber. 1986. Atomic force microscope. *Phys. Rev. Lett.* 56:930–933.

Bustamante, C., J. Vesenka, C. L. Tang, W. Rees, M. Guthold, and R. Keller. 1992. Circular DNA molecules imaged in air by scanning force microscopy. *Biochemistry.* 31:22–26.

Cleveland, J. P., S. Manne, D. Bocek, and P. K. Hansma. 1993. A nondestructive method for determining the spring constant of cantilevers for scanning force microscopy. *Rev. Sci. Instrum.* 64:403–405.

DeMey, J. 1984. Colloidal gold as marker and tracer in light and electron microscopy. *EMSA Bull.* 14:54–66.

Drake, B., C. B. Prater, A. L. Weisenhorn, S. A. C. Gould, T. R. Albrecht, C. F. Quate, D. S. Cannell, H. G. Hansma, and P. K. Hansma. 1989. Imaging crystals, polymers, and processes in water with the atomic force microscope. *Science (Wash. DC).* 243:1586–1589.

Engel, A. 1991. Biological applications of scanning probe microscopes. *Annu. Rev. Biophys. Chem.* 20:79–108.

Frens, G. 1973. Controlled nucleation for the regulation of the particle size in monodisperse gold solutions. *Nature (Lond.).* 241:20–22.

Giles, R., J. P. Cleveland, S. Manne, P. K. Hansma, P. Maivald, C. Boles, J. Gurley, and V. Elings. 1993. Non-contact force microscopy in fluids. *Appl. Phys. Lett.* 63(5).

Hansma, H., J. Vesenka, C. Siegerist, G. Kelderman, H. Morret, R. L. Sinsheimer, V. Elings, C. Bustamante, and P. K. Hansma. 1992a. Reproducible imaging and dissection of plasmid DNA under liquid with the atomic force microscope. *Science (Wash. DC).* 256:1180–1184.

Hansma, H. G., R. L. Sinsheimer, M.-Q. Li, and P. K. Hansma. 1992b. Atomic force microscopy of single- and double-stranded DNA. *Nucleic Acids. Res.* 20:3585–3590.

Henderson, E., P. G. Haydon, and D. S. Sakaguchi. 1992. Actin filament dynamic in living glial cells imaged by atomic force microscopy. *Science (Wash. DC).* 257:1944–1946.

Keller, D. 1992. Reconstruction of STM and AFM images distorted by finite-size tips. *Surface Sci.* 253:353–365.

Keller, D., and C. Chih-Chung. 1992. Imaging steep, high structures by scanning force microscopy with electron beam deposited tips. *Surface Sci.* 268:333–339.

Y., and S. M. Lindsay. 1991. Polystyrene latex particles as a size calibration for the atomic force microscope. *Rev. Sci. Instrum.* 62:2630–2633.

Lyubchenko, Y. L., B. L. Jacobs, and S. Lindsay. 1992. Atomic force microscopy of reovirus dsRNA: a routine technique for length measurements. *Nucleic Acids Res.* 20:3983–3986.

Lyubchenko, Y. L., P. I. Oden, D. Lampner, S. M. Lindsay, and K. A. Dunker. 1993. Atomic force microscopy of DNA and bacteriophage in air, water and propanol: the role of adhesion forces. *Nucleic Acids Res.* 21:1117–1123.

Maivald, P., H. J. Butt, S. A. C. Gould, C. B. Prater, B. Drake, J. A. Gurley, V. B. Elings, and P. K. Hansma. 1991. Using force modulation to image surface elasticities with the atomic force microscope. *Nanotechnology.* 2:103.

Mathews, R. E. F. 1981. Plant Virology. 2nd ed. Academic Press, New York. 725.

Mühlpfordt, H. 1982. The preparation of colloidal gold particles using tannic acid as an additional reducing agent. *Experientia.* 38:1127–1128.

Putman, C. A. J., K. van der Werk, B. G. de Grooth, N. F. van Hulst, J. Greve, and P. K. Hansma. 1992. A new imaging mode in atomic force microscopy based on the error signal. *SPIE Conf. Proc.* 1639:198–204.

Putman, C. A. J., B. G. deGrooth, P. K. Hansma, N. K. van Hulst, and J. Greve. 1993. Immunogold labels: cell-surface markers in atomic force microscopy. *Ultramicroscopy.* 48:177–182.

Radmacher, M., R. W. Tillmann, M. Fritz, and H. E. Gaub. 1992. From molecules to cells: imaging soft samples with the atomic force microscope. *Science (Wash. DC).* 257:1900–1905.

Shaiu, W.-L., D. D. Larson, J. Vesenka, and E. Henderson. 1993a. Atomic force microscopy of oriented linear DNA molecules labeled with 5 nm gold spheres. *Nucleic Acids Res.* 21:99–103.

Shaiu, W.-L., J. Vesenka, D. Jondle, E. Henderson, and D. D. Larson. 1993b. Visualization of circular DNA molecules labeled with colloidal gold spheres using atomic force microscopy. *J. Vac. Sci. Technol. A.* In press.

Slot, J. W., and H. J. Geuze. 1985. A new method of preparing gold probes for multiple labeling cytochemistry. *Eur. J. Cell Biol.* 38:87.

Thundat, T., X.-Y. Zheng, S. L. Sharp, D. P. Allison, R. J. Warmack, D. C. Joy, and T. L. Ferrell. 1992a. Calibration of atomic force microscope tips using biomolecules. *Scanning.* 6:903–910.

Thundat, T., R. J. Warmack, D. P. Allison, A. J. Lourenco, and T. L. Ferrel. 1992b. Atomic force microscopy of deoxyribonucleic acid strands adsorbed on mica: the effect of humidity on apparent width and image contrast. *J. Vac. Sci. Technol. A.* 10:632–635.

Vesenka, J., C. L. Tang, M. Guthold, D. Keller, E. Delaine, and C. Bustamante. 1992a. A substrate preparation for reliable imaging of DNA molecules with the scanning force microscope. *Ultramicroscopy.* 42–44: 1243–1249.

Vesenka, J., H. Hansma, C. Siegerist, G. Siligardi, E. Schabtach, and C. Bustamante. 1992b. Scanning force microscopy of circular DNA and chromatin in air and propanol. *SPIE Conf. Proc.* 1639:127–137.

Yang, J., and Z. Shao. 1993. The effect of probe force on the resolution of atomic force microscopy of DNA. *Ultramicroscopy.* In press.

Zasadzinski, J. A. N., C. A. Helm, M. L. Longo, A. L. Weisenhorn, S. A. C. Gould, and P. K. Hansma. 1991. Atomic force microscopy of hydrated phosphatidylethanolamine bilayers. *Biophys. J.* 59:755–760.

Zenhausern, F., M. Adrian, B. ten Heggeler-Bordier, L. M. Eng, and P. Descouts. 1992a. DNA and RNA polymerase/DNA complex imaged by scanning force microscopy: influence of molecular-scale friction. *Scanning.* 14:212–217.

Zenhausern, F., M. Adrian, B. ten Heggeler-Bordier, R. Emch, M. Jobin, M. Taborelli, and P. Descouts. 1992b. Imaging of DNA by scanning force microscopy. *J. Struct. Biol.* 108:69–73.